Dilution of Individual Microtubules Observed in Real Time In Vitro: Evidence That Cap Size Is Small and Independent of Elongation Rate

R. A. Walker, N. K. Pryer, and E. D. Salmon

Department of Biology, University of North Carolina, Chapel Hill, North Carolina 27599-3280

Abstract. Although the mechanism of microtubule dynamic instability is thought to involve the hydrolysis of tubulin-bound GTP, the mechanism of GTP hydrolysis and the basis of microtubule stability are controversial. Video microscopy of individual microtubules and dilution protocols were used to examine the size and lifetime of the stabilizing cap. Purified porcine brain tubulin (7–23 μM) was assembled at 37°C onto both ends of isolated sea urchin axoneme fragments in a miniature flow cell to give a 10-fold variation in elongation rate. The tubulin concentration in the region of microtubule growth could be diluted rapidly (by 84% within 3 s of the onset of dilution). Upon perfusion with buffer containing no tubulin, microtubules experienced a catastrophe (conversion from elongation to rapid shortening) within 4–6 s on average after dilution to 16% of the initial concentration, independent of the predilution rate of elongation and length. Based on extrapolation of catastrophe frequency to zero tubulin concentration, the estimated lifetime of the stable cap after infinite dilution was <3–4 s for plus and minus ends, much shorter than the ≈200 s observed at steady state (Walker, R. A., E. T. O'Brien, N. K. Pryer, M. Soboeiro, W. A. Voter, H. P. Erickson, and E. D. Salmon. 1988. *J. Cell Biol.* 107:1437–1448.).

We conclude that during elongation, both plus and minus ends are stabilized by a short region (≈200 dimers or less) and that the size of the stable cap is independent of 10-fold variation in elongation rate. These results eliminate models of dynamic instability which predict extensive "build-up" stabilizing caps and support models which constrain the cap to the elongating tip. We propose that the cell may take advantage of such an assembly mechanism by using "catastrophe factors" that can promote frequent catastrophe even at high elongation rates by transiently binding to microtubule ends and briefly inhibiting GTP-tubulin association.

INDIVIDUAL microtubules reassembled from purified tubulin undergo alternating phases of elongation and rapid shortening (19, 26, 49). The transition (catastrophe) from elongation to rapid shortening, and the reverse transition (rescue), are abrupt, stochastic, and occur infrequently in comparison to the rates of subunit association and dissociation (49). This behavior, termed dynamic instability (26), is also exhibited by the majority of microtubules in the mitotic spindle and the interphase cytoplasmic microtubule complex (CMTC)[1] (12–14, 33–36, 38, 39) and appears necessary for chromosome–spindle attachment, chromosome segregation, cellular morphogenesis, and establishment of cell polarity (13, 17, 21, 29–32). Changes in frequencies of catastrophe and rescue between mitosis and interphase are thought to convert the dynamic, short microtubule arrays of the mitotic spindle into the long, less dynamic array of the interphase CMTC (3, 12, 14, 17, 36, 43, 47). Although it has been shown that the kinase activity of the cell cycle regulator, $p34^{cdc2}$, regulates changes in dynamic instability between mitosis and interphase (3, 43), little information is available regarding the regulatory factors that may interact directly with microtubules.

Fundamental to this problem is the molecular basis of dynamic instability, which though unresolved at present, is thought to depend on a "stable cap/labile core" mechanism. Elongation-competent subunits add to a growing microtubule end and experience a destabilizing conformational change subsequent to assembly. This conformational change produces an interior "core" of labile subunits stabilized at the microtubule end by continually adding elongation-competent subunits (the stable cap). In this model, catastrophe is produced by stochastic loss of the terminal stable subunits either by conformational change or dissociation. Rescue oc-

R. A. Walker's current address is Department of Cell Biology, Duke University Medical Center, Durham, NC 27710. N. K. Pryer's current address is Department of Biochemistry, University of California, Berkeley, CA 94720.

1. *Abbreviation used in this paper*: CMTC, cytoplasmic microtubule complex.

curs if the stable cap reforms before a microtubule shortens to completion.

Although the nature of the stabilizing cap is controversial, there is strong evidence for a stable cap/labile core model and that GTP hydrolysis is somehow involved (6, 7, 19, 26, 49, 50). Evidence to date indicates that GTP-tubulin dimers serve as the stabilizing, elongation-competent subunits and that the hydrolysis of the bound GTP to GDP after assembly leads directly or indirectly to the destabilization of the dimer within the microtubule lattice (6, 9, 16, 23, 27, 51). The stabilizing cap may simply be GTP–tubulin (5, 6, 9, 10, 22, 26, 28). However, Carlier and co-workers (11, 25) have proposed that P_i release after hydrolysis is slow relative to tubulin association and the stable cap consists of both GTP– and GDP-P_i–tubulin. Alternatively, Stewart et al. (41) have proposed that the conversion from stable to instable dimer lags behind hydrolysis, so that the end of a microtubule could have a small GTP or GDP-P_i cap, but an extensive, conformationally stable cap. A region at the growing end of a microtubule is clearly capable of stabilizing an entire microtubule (7, 49, 50), but the actual amount of GTP-tubulin, GDP-P_i-tubulin, and/or conformationally stable tubulin present at the end has remained below the limit of detection (27, 37, 41).

Existing cap models can be divided into two classes: (*a*) uncoupled destabilization models, which specify no direct link between tubulin subunit addition and destabilization; and (*b*) coupled destabilization models, which link destabilization to subunit addition. For uncoupled models, destabilization has been postulated to be stochastic, i.e., any GTP–tubulin may be destabilized, regardless of its location in the polymer lattice (9, 26); vectorial, i.e., destabilization is promoted at a GDP–tubulin:GTP–tubulin interface within the microtubule lattice (5, 10) or a combination of stochastic and vectorial mechanisms (15). In contrast, coupled destabilization models propose that destabilization occurs when the subunit becomes buried in the microtubule lattice through addition of another subunit (1, 27, 49). Uncoupled models can produce substantial "build-up" caps at higher rates and durations of elongation (5, 10, 28; Voter, W. A., E. T. O'Brien, and H. P. Erickson. 1987. *Biophys. J.* 51:214a), whereas coupled models predict that cap size is small and essentially independent of elongation rate and duration (1, 27, 49).

Information about the size of the stabilizing cap can be obtained from dilution-induced disassembly experiments. The delay from the time of dilution to the time of catastrophe provides a measure of cap size since the delay time reflects the time required for loss of stable subunits (by hydrolysis and/or dissociation) from the microtubule end. If microtubules are assembled over a range of tubulin concentrations, one could determine whether this delay after dilution is a function of the predilution microtubule elongation rate, and therefore discriminate between uncoupled and coupled destabilization models based on each model's predicted response to dilution of the free tubulin pool. Uncoupled models predict that microtubules assembled at higher tubulin concentrations, and hence greater elongation rates, will take longer to convert to rapid shortening since these microtubules have longer caps. In contrast, coupled models predict that, regardless of the tubulin concentration and predilution elongation rate, all microtubules will take approximately the same time to convert to rapid shortening.

In this paper, video microscopy and dilution protocols were used to measure directly the life-time of the stabilizing cap at the ends of individual microtubules after tubulin association was abruptly inhibited. Purified tubulin (7–23 μM) was assembled at 37°C onto the plus and minus ends of axoneme seeds attached to the inner surfaces of the glass windows of a miniature flow cell (4). The flow cell was specifically designed to produce laminar flow and to be used with the high-power microscope objectives required for video-enhanced differential interference contrast (VE-DIC) microscopy. Following assembly, microtubules were rapidly diluted by perfusion with microtubule reassembly buffer without tubulin, or reassembly buffer containing either 2 or 3.3 μM tubulin. Dilution at the window surface in the flow cell is not instantaneous, and depends on diffusion as well as flow rate (4). We determined that molecules the size of tubulin will be diluted to nearly 15% of the initial concentration within 3 s after initiation of dilution with reassembly buffer. Although the spontaneous frequency of catastrophe at both ends becomes infrequent at higher rates of tubulin association (49), we found that, for both ends, the lag between dilution and catastrophe was several seconds at low tubulin concentrations, and was independent of predilution elongation rate and length.

Materials and Methods

Tubulin and Axoneme Preparation

Phosphocellulose-purified porcine brain tubulin was prepared as described previously (44, 49). The final tubulin pellets were resuspended in PM buffer (100 mM Pipes, 2 mM EGTA, 1 mM $MgSO_4$, pH 6.9) containing 1 mM GTP (PM/GTP), passed over a G-25 Sephadex column equilibrated with PM/GTP, and frozen in small aliquots. Microtubule-associated proteins constituted no more than 0.6% of the purified tubulin preparation (49). Axoneme fragments were prepared from *S. purpuratus* (2, 49).

Flow Cell Construction and Calibration

The flow cell used in this study was identical to that described by Berg and Block (4). Coverslips were sealed to the cell with a thin layer of high-vacuum grease (Dow Corning, Midland, MI) and the edges were further sealed with Valap (a 1:1:1 mixture of petrolatum, lanolin, and beeswax). The distance between inner coverslip surfaces was ~350 μm. A short piece of Intramedic PE-60 polyethylene tubing (Clay Adams, Parsippany, NJ) was slipped over the inlet pipe so that a 1-cm length of tubing extended beyond the inlet pipe. The cell was filled with PM from the inlet side, and then backfilled from the outlet side to remove air from the inlet pipe. After placement on the microscope stage, the outlet tubing was slipped over the outlet pipe. The rate of flow was controlled by a peristaltic pump (Isco Tris pump; Isco, Inc., Lincoln, NE), and an Apple II computer was used to control the pump and duration of flow.

Observing individual microtubules in the flow cell during dilution required that the microtubules (particularly the ends) remain relatively stationary. Self-assembled microtubules invariably were swept from the field of view by flow, so axoneme fragments, which adhered to the glass surfaces of the flow cell, were used to nucleate microtubule growth. As events were constrained to the region near the glass surfaces of the chamber, and image quality was marginal at the inner surface of the lower coverslip, it was necessary to determine the rate of dilution specifically in the region just inside the inner surface of the upper coverslip. This was done using a confocal measurement system to record the fluorescent emission of a reporter molecule. A Zeiss Standard microscope was equipped with a IV FL epi-illuminator, fluorescein filter set, and a 100-W mercury arc lamp as the excitation source. An 0.3-mm-diam aperture was placed at the field diaphragm plane of the epi-illuminator. A Nikon 100×/1.40 NA PlanApo objective projected a 3-μm spot onto the specimen plane and collected the resultant fluorescent emission. The specimen image was projected to a 0.75-mm diaphragm aperture and the fluorescence that passed this diaphragm was measured by a pho-

tomultiplier (EMI 9863A, Thorn EMI Gencom, Inc.) and photon counter (EMI model C-10). This diaphragm arrangement limited the contribution of out-of-focus fluorescence from distances ≥10 μm away to <15%.

The rate of dilution was a reflection of: (*a*) the rate of flow; (*b*) the duration of flow; and (*c*) the diffusion properties of the molecule of interest. In our experiments, a flow rate of 0.014 ml/s was used since at greater flow rates, microtubules frequently broke off at the axoneme and were swept from the field of view. Flow times (6–8 s) were selected to be long enough to give significant dilution but short enough not to interfere with visualization of the transition to rapid shortening and the shortening process itself. Fluorescein-BSA (Molecular Probes, Eugene, OR) and fluorescein dextran (60,000–90,000 mol wt; Polysciences, Inc., Warrington, PA) were used as reporter molecules because they were of comparable size and have similar diffusion coefficients to tubulin. Both were suspended in PM and passed over a Sephadex G-25 column to remove free dye. We attempted to calibrate the kinetics of tubulin dilution in the flow cell using tubulin labeled with 5-(4,6-dichlorotriazin-2-yl) amino fluorescein (DTAF) (24, 48). However, we found that DTAF-tubulin heavily coated the coverslip surface (when viewed by VE-DIC microscopy) and gave anomalous dilution profiles. Neither purified tubulin, fluorescein-BSA, nor fluorescein-dextran noticeably coated the coverslip surface, and both fluorescein-BSA and fluorescein-dextran gave consistent and similar dilution profiles.

For calibration experiments, the flow cell was assembled and placed on the microscope as described above. Temperature on the microscope stage was maintained at 37°C by an air curtain incubator (model 279, Sage; Orion Research, Inc., Cambridge, MA). Intensity measurements were made 2.5 μm below the inner surface of the upper coverslip since this was the region of microtubule growth. Labeled BSA or dextran at 1 or 2.2 mg/ml was washed in, and the chamber centered close to the optical axis. To mimic experiments performed with tubulin, the reporter molecule was then washed out with one of the following: (*a*) PM buffer; (*b*) 0.2 mg/ml reporter molecule in PM; or (*c*) 0.33 mg/ml reporter in PM. Intensity values were recorded at 0.1-s intervals. After the majority of fluorescence had been diluted (typically 8 s after flow was initiated), the excitation source was shuttered on a 0.8-s open/2.4-s closed cycle to limit photobleaching of immobile, coverslip-bound fluorescence. Intensity values and the time at which the pump was switched on were saved in an Apple II computer.

The characteristic dilution profile exhibited three phases: (*a*) an ~3-s delay during which the initial concentration remained unchanged; (*b*) an ~3–5-s period during which the reporter molecule was diluted approximately fivefold; and (*c*) an extended period of time during which reporter molecules continued to diffuse out of the near-coverslip region. Rate of dilution curves were plotted using the following equation:

$$\text{Relative Intensity} = (F(t) - F_\infty) / (F_I - F_\infty)$$

where $F(t)$ is the photon count measured at a given time, F_∞ is the average photon count at infinity (contributed by the immobile fraction), and F_I is the average predilution photon count. Typically, 20–30 points were averaged to obtain F_I, 15–25 points were averaged to obtain F_∞, and F_∞ was 5–15% of F_I. Two successive flows were performed to ensure complete dilution and to determine F_∞ accurately. Dilution profiles of fluorescein-BSA and fluorescein–dextran were indistinguishable and were averaged together in Figs. 4 and 5.

Dilution Experiments

Individual microtubules were observed at 37°C by the methods of Walker et al. (49). Once the cell was assembled, placed on the microscope stage, and oil contacted to the objective and condenser, axonemes (at ~2.7×10^7/ml) were flushed into the cell and allowed to remain for 5–10 min to attach to the glass surfaces of the cell. PM buffer was then run through the cell to remove unattached axonemes. Tubulin (7–23 μM active tubulin in PM/GTP) was drawn into the chamber and microtubule assembly onto axoneme fragments was observed. The diluent was prepared (containing 0, 2, or 3.3 μM tubulin in PM/GTP) and warmed to 37°C in a nearby temperature bath. When microtubules were long enough to visualize clearly but did not yet extend beyond the field of view, the diluent was quickly placed over the inlet tubing and the pump was switched on. Focus was maintained on the shifting microtubules during the flow.

Microtubule dynamics were analyzed using previously published procedures (49). Delay values (to the nearest second) were determined by reading the time from the date-time generator. The initiation of flow and of rapid shortening were identified visually with the aid of the videocassette recorder's search control.

Results

Catastrophe Is Induced by Tubulin Dilution

In our initial studies, microtubules were grown in PM/GTP buffer at 20 μM tubulin. Upon perfusion, the longer microtubules, particularly those oriented toward the inlet side of the flow cell, were bent by the flow. Such perturbation occasionally made visualization of microtubule ends impossible during perfusion, but based on control experiments in which the tubulin concentration was kept constant, perfusion did not induce catastrophe (data not shown). In contrast, catastrophe occurred quickly after perfusion with PM/GTP buffer without tubulin (Fig. 1). The delays from the time at which flow was initiated to the time at which rapid shortening began were short, but variable between individual microtubules. Delays varied within a given field-of-view, for microtubules assembled onto the same axoneme, and for microtubule ends near each other. For example, Fig. 2 shows the dynamic histories of three microtubules in the same field-of-view. Each microtubule began shortening at a different time, and two minus end microtubules had delays of 6 and 40 s. During delays, no change in microtubule length was measurable within the limit of accuracy of our analysis system (~0.25 μm or 400 tubulin dimers), even for the microtubules which showed the longest delays.

Delays before Catastrophe Are Independent of Predilution Elongation Rate and Microtubule Length

To determine if delay times depended on predilution microtubule elongation rate or length, tubulin subunits were assembled onto axoneme fragments over a range of tubulin concentrations (7–23 μM) and then diluted with PM/GTP. Delays ranged from 3 to 25 s for the plus end, and from 2 to 44 s for the minus end. Linear regression analysis indicated that there was no significant correlation between delay time and predilution elongation rate for either plus ($r = 0.15$; $n = 147$) or minus end ($r = 0.12$; $n = 122$) microtubules (Fig. 3). There was also no significant correlation between delay time and predilution microtubule length for either plus ($r = 0.09$) or minus end ($r = 0.10$) microtubules (Fig. 3).

When delay times for each end were compared with the dilution calibration curve, it was evident that most microtubules did not convert to rapid shortening until after the bulk of dilution was complete (at 8 s, see Fig. 4). Therefore, delays in the 2–3-s range probably represent microtubules that converted spontaneously to rapid shortening during dilution. The mean delays between significant dilution (at 8 s) and catastrophe were 4.2 ± 3.6 and 6.1 ± 6.7 s for the plus and minus ends, respectively. Based on the dilution calibration curve, the initial tubulin concentration was diluted to nearly 16% of its original value by 8 s, and the level continually dropped as free tubulin subunits diffused from the region near the coverslip surface. Percentage of dilution did not vary with the initial concentration, so that the 16% tubulin concentration estimate after dilution ranged from 1.1 to 3.7 μM tubulin, depending on the initial tubulin concentration (7–23 μM).

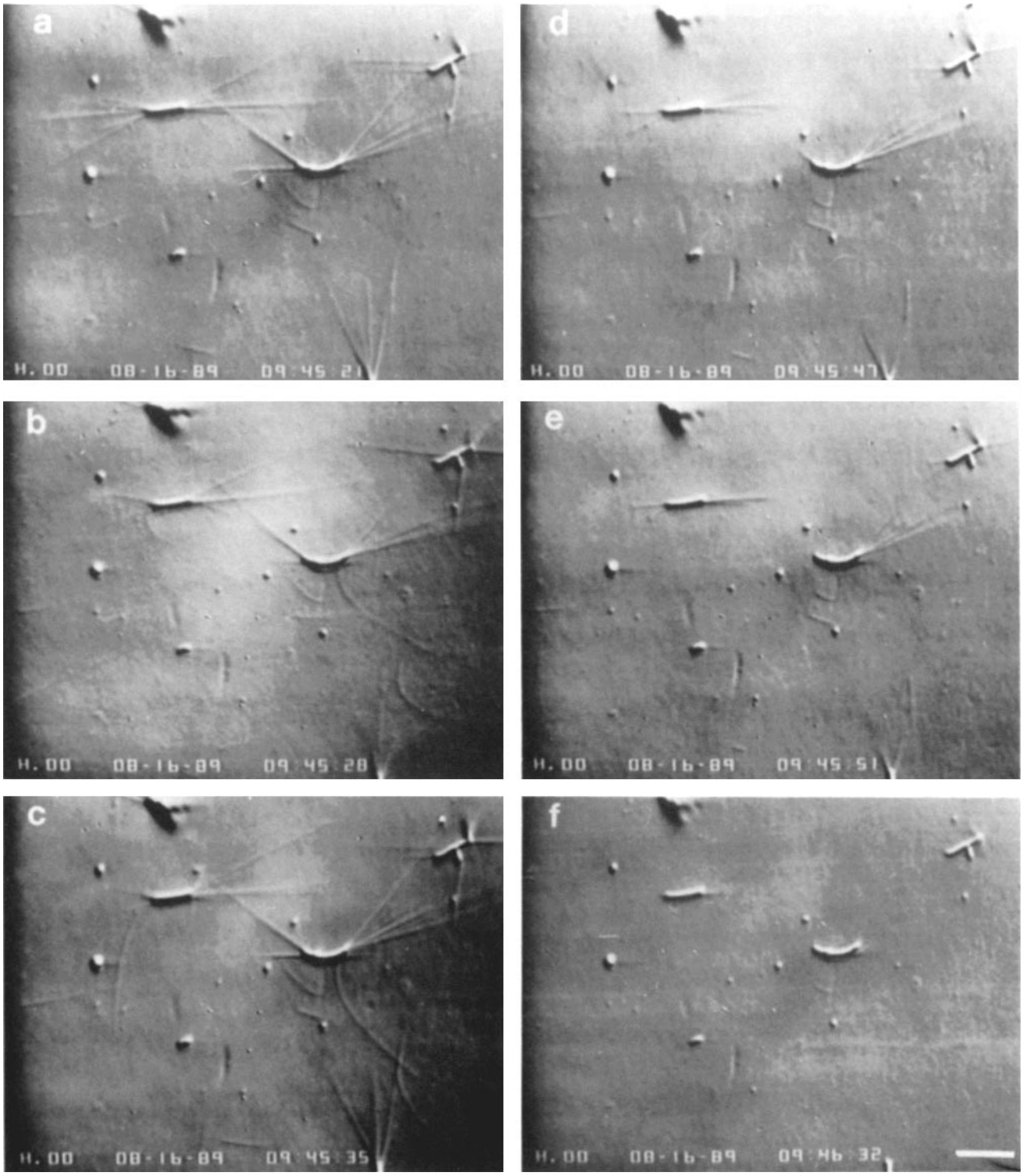

Figure 1. Microtubule dilution observed in real time. Microtubules were assembled at 20 μM tubulin. PM/GTP and no tubulin was drawn into the chamber at 9:45:25. Flow was stopped at 9:45:33. Most microtubules are in the rapid shortening phase by 9:45:47 and some have already shortened to completion. Flow is from left to right across the field. Bar, 5 μm.

Catastrophe Occurs Within Seconds Near Zero Tubulin Concentration

The above results show that catastrophe occurs within several seconds when the free tubulin concentration is diluted below the critical concentration for elongation, (S_c^e, which is ~5 μM for both ends [ref. 49]). This is much quicker than for tubulin concentrations above S_c^e, where the balance of association and dissociation reactions favor elongation (at 7 μM, microtubules elongate for ~200 s on average; at 15 μM, they persist for ~1,000 s). To obtain information about

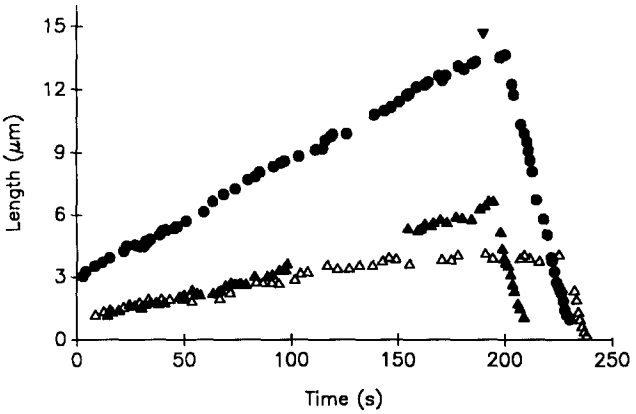

Figure 2. Dynamic histories of individual microtubules diluted with PM buffer. Plots of microtubule length versus time are presented for three microtubules during the same dilution experiment. Perfusion was initiated at 190 s (*arrow*) and continued for 6 s. A plus end microtubule (*closed circles*) experiences a delay of 12 s, whereas two different minus end microtubules experience delays of 6 s (*closed triangles*) and 40 s (*open triangles*). The minus end microtubule indicated by the closed triangles was obscured by an adjacent microtubule from 100 to 150 s. The limit of accuracy was ~0.25 μm, except during flow, when accuracy greatly (0.25 μm to immeasurable) varied depending on the orientation relative to the direction of flow of the microtubule and the distance the microtubule extended into the chamber.

the stability of microtubules at tubulin concentrations below S_c^e, microtubules were assembled in the presence of 20–23 μM tubulin and then perfused with PM/GTP buffer containing either 2 or 3.3 μM tubulin. Microtubules perfused with 2 μM tubulin had delays similar to those measured after perfusion with PM/GTP (data not shown), but shorter delays than microtubules perfused with 3.3 μM tubulin (Fig. 5). Delays after the start of perfusion with 2 and 3.3 μM tubulin were 8–19 s and 7–41 s for the plus end, and 7–36 s and 11–74 s for the minus end. After the bulk of dilution was completed (at 8 s), the average delay before rapid shortening was 5.0 ± 3.0 s (n = 21) vs. 10.8 ± 7.5 s (n = 54) for the plus end and 7.6 ± 5.5 (n = 28) vs. 24.2 ± 18 (n = 47) for the minus end. Based on the dilution calibration curves, most microtubules perfused with 2 μM tubulin converted to rapid shortening while the free tubulin concentration was dropping from 16% (at 8 s) to 14% (final) of its initial value, or from ~3.4 to ~3 μM tubulin. For perfusion with 3.3 μM tubulin, most microtubules converted while the free tubulin concentration dropped from 23% (at 8 s) to 21% (final) of the initial value, or from ~4.9 to ~4.5 μM tubulin.

Microtubule lifetime at zero tubulin concentration was estimated by extrapolation of logarithmic plots of catastrophe frequency versus tubulin concentration (Fig. 6). Catastrophe frequencies below S_c^e were obtained from the reciprocal of the delays measured above for tubulin dilution to 3–3.4 μM and 4.5–4.9 μM, whereas those above S_c^e were obtained

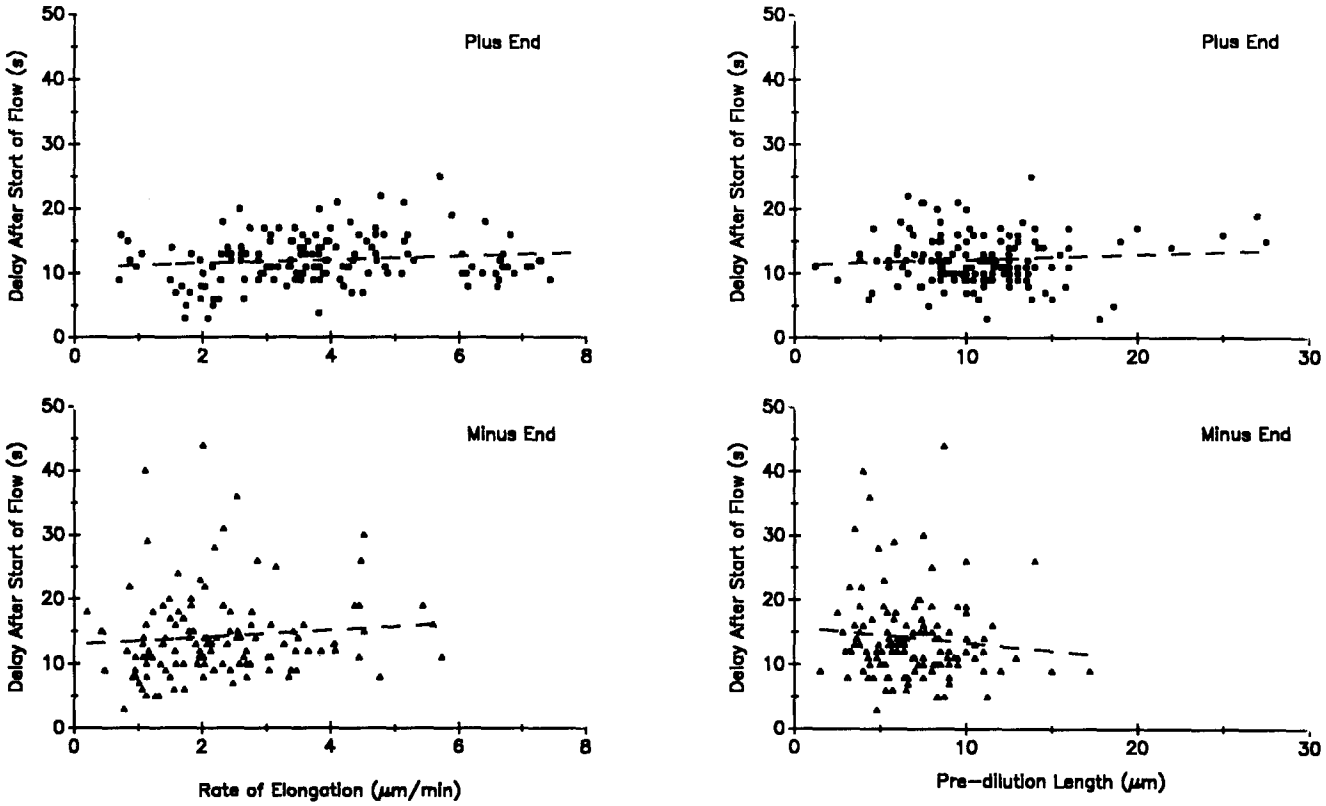

Figure 3. Delay in the onset of dilution-induced rapid shortening as a function of the predilution elongation rate and microtubule length for plus and minus end microtubules. Microtubules were assembled onto axoneme fragments in the presence of 7–23 μM free tubulin and diluted with PM/GTP for 6 or 8 s. Delay values represent the interval from start of perfusion until conversion to rapid shortening. Data obtained from 6- and 8-s dilutions were not significantly different (independent t test). The slopes (*dashed lines*) were determined by linear regression analysis. There was no significant correlation between the delay in the onset of rapid shortening and the predilution elongation rate or microtubule length for either plus or minus end microtubules.

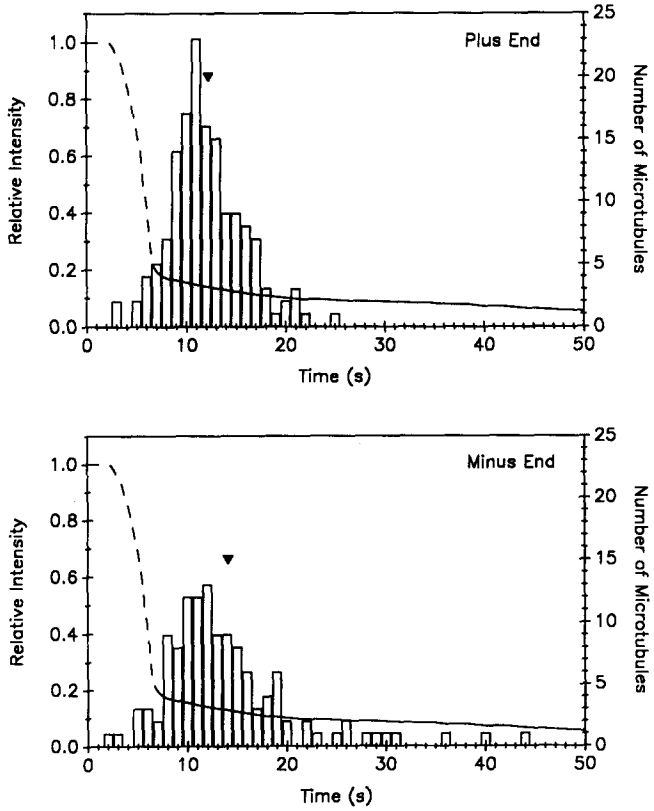

Figure 4. Comparison of the near-surface dilution profile and the delays in the onset of rapid shortening. Data set from Fig. 3. The mean delays from the start of flow to the onset of rapid shortening are indicated by the arrowheads. The rate of dilution was determined as described in Materials and Methods. The 6-s flow curve is shown, but the 8-s curve was not significantly different. While flow was occurring, we were unable to measure intensity values accurately, since suction produced by the pump pulled the upper coverslip inward by ≈2 μm and the relative contribution of out-of-focus fluorescence was altered during this time, i.e., the fluorescence between the plane of focus and the coverslip surface was decreased. The dashed portion of the curve indicates estimated values based on measurements 5 μm below the coverslip's inner surface, and the solid portion represents data for the region 2.5 μm below the coverslip's inner surface.

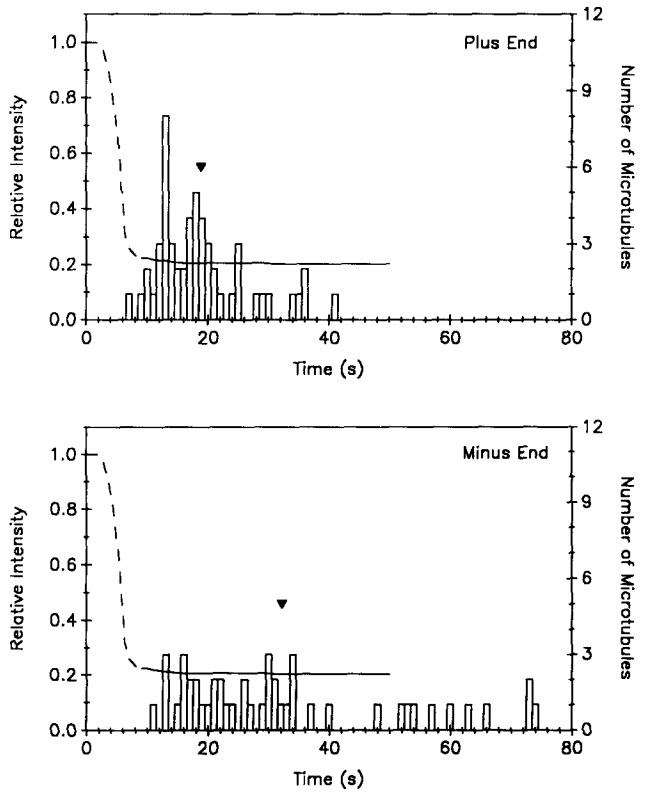

Figure 5. Comparison of the near-surface dilution profile and the delays in the onset of rapid shortening for microtubules assembled at 20–23 μM free tubulin and then diluted with 3.3 μM tubulin in PM/GTP for 8 s. The mean delays from the start of flow to the onset of rapid shortening are indicated by the arrowheads. The dilution profile is as in Fig. 4, but is based on calibrations using 0.33 mg/ml reporter molecule.

from the previous study of Walker et al. (49). Extrapolation to zero concentration yields catastrophe frequencies of 1/3 s^{-1} for the plus end and 1/4 s^{-1} for the minus end.

Other Observations Related to Dynamic Instability

It has been demonstrated that, for tubulin concentrations above S_c^e, the rate of rapid shortening of plus ends is slower than minus ends, and that for both ends, the rates are independent of tubulin concentration (49). We measured the rapid shortening rates of the microtubules after dilution below S_c^e, and found that plus end microtubules shortened at 33 ± 1 μm/min (SEM; n = 210), whereas minus end microtubules shortened at 46 ± 2 μm/min (SEM; n = 156), values typical of tubulin concentrations above S_c^e (49).

In addition, it was argued previously by Walker et al. (49) that rescue will not occur for tubulin concentrations below S_c^e since dissociation is favored and net elongation does not

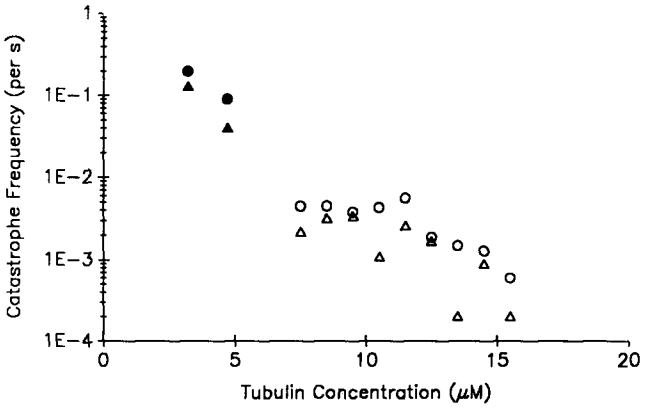

Figure 6. Frequency of catastrophe below S_c^e. From the delays observed in dilutions with 2 and 3.3 μM tubulin, and the estimated tubulin concentrations at which the majority of microtubules converted to rapid shortening, catastrophe frequencies were estimated for dilution to ≈3.4–3.0 and ≈4.9–4.5 μM tubulin (*closed symbols*). The symbol width approximates the concentration range in each case. Open symbols represent data from Fig. 7 of Walker et al. (49). Plus end data are indicated by circles, minus end data are indicated by triangles.

occur. To test this hypothesis, we looked for rescue events in our dilution studies. After dilution below S_c^e, no rescue events were observed for the 210 plus end and 165 minus end microtubules analyzed during rapid shortening.

Discussion

The Short Stable Cap Is Constrained to the Tip of an Elongating Microtubule

The main findings in our studies are that after dilution from 7–23 μM to near zero free tubulin, the mean time of conversion to rapid shortening for both the plus and minus ends was only a few seconds and was independent of predilution elongation rates of 10–200 dimers/s and lengths of 4,000–44,000 dimers. Given these results and the predictions of each class of models (see Introduction), tubulin subunit destabilization must be coupled in some way to subunit addition. Uncoupled models that predict an extensive "build-up" cap (5, 9, 10, 11, 25, 26, 28; Voter, W. A., E. T. O'Brien, and H. P. Erickson. 1987. *Biophys J.* 51:214a) or models that combine coupled hydrolysis with long, stabilizing conformational caps (41) can be ruled out. Before discussing the various instability models, it is worth considering the life-time and size of the cap.

Extrapolation of the catastrophe data in Fig. 6 to zero tubulin yielded delays of 3 and 4 s for the plus and minus ends. These are first approximation values since the extrapolation assumes that catastrophe frequency depends exponentially upon tubulin concentration, an assumption that gives a reasonable fit to the data. These values are consistent with the recent studies of Voter et al. (46), who diluted a steady-state microtubule population 15-fold (to a free subunit concentration of ~0.5 μM) and found that microtubules converted to rapid shortening within ~1 s. Shearing can induce rapid shortening of severed plus ends within a second of cutting (50), a factor which may contribute to the difference between our 3–4-s estimates and the 1 s measured by Voter et al. (46). Alternatively, since catastrophe frequency depends on tubulin concentration (Fig. 6; reference 49) and dilution in the flow cell is not instantaneous, it is possible that more rapid and complete dilution would yield values closer to 1 s. Nevertheless, it is clear that when elongation is abruptly blocked, the mean life-time of the stabilizing cap is on the order of a second.

Since catastrophe occurs within a few seconds of dilution, the number of dimers stabilizing an end must be small. When tubulin association is blocked, stable dimers can disappear from the cap by dissociation and/or conversion to labile dimers. The rate of dissociation during elongation has been calculated to be 44 and 23 dimers/s for the plus and minus ends (49). If the conversion of stable to unstable dimers (GTP hydrolysis and conformational change) is coupled to elongation, then, after dilution to zero tubulin, the cap is lost only by dissociation. If uncoupled conversion also contributes to cap loss, the rate of uncoupled conversion cannot be any greater than the growth rate at 7 μM tubulin, 18 dimers/s, an association rate that sustains elongation for ~200 s before a catastrophe occurs. These values and the 3- and 4-s delays measured in our experiments give upper limits to the number of stable dimers in the cap of 132 for the plus ends and 92 for the minus ends without uncoupled conversion and 186 and 164, respectively, with uncoupled conversion. The 1-s delay measured by Voter et al. (46) would decrease these values by one-third and one-fourth, respectively. Regardless, our dilution studies yield an upper limit of ~100–200 dimers in the stable cap, independent of growth rate and duration over the tubulin concentrations typical of living cells (18). A cap size of ~100–200 subunits or less is also consistent with reports which have used biochemical methods to estimate the amount of GTP- or GDP-P_i–tubulin at the end of a microtubule (27, 37, 41).

Implications for Stable Cap Models

Carlier and co-workers (9, 10, 11, 25, 28) have reported lags between microtubule assembly, GTP hydrolysis, and P_i release. In initial studies (9), they reported that GTP hydrolysis and formation of labile dimer (k_l) occurred at 0.004/s, and proposed that destabilization was a stochastic process independent of tubulin association rate and position in the microtubule lattice. Recently, they have revised their measurements of GTP hydrolysis to a value ~10-fold higher, and have also proposed that stochastic P_i release (at 0.02/s) is the rate limiting step in the formation of labile GDP-tubulin (25). Consider, for example, plus end growth for 180 s at 7 and 23 μM tubulin, which would produce microtubules of 3,240 and 28,980 dimers respectively. A value of k_l = 0.02/s yields stable caps of 875 and 7,845 subunits, where the number of stable subunits in the cap after elongation to length (L) in time (t) is given by $L(1 - e^{-k_l t})/(k_l t)$ (28). These caps are considerably larger than the 100 dimers determined from our experiments, and predict minimum delays of 17 and 75 s at zero free tubulin, assuming stochastic P_i release (at 0.02/s) and dissociation of terminal GTP-tubulin subunits (at 44/s) continues.

Our results also rule out any type of uncoupled, vectorial destabilization model (5, 10). In this model, labile GDP–tubulin is generated by hydrolysis alone or by subsequent P_i release at interfaces distal from the growing microtubule end at rates independent of the rate of tubulin association. After initiation of elongation, a stable cap builds up at a rate equal to the difference between the rate of labile GDP–tubulin formation, k_l, and the rate of tubulin association. Consider again plus end elongation at 7 and 23 μM tubulin for 180 s. To keep the cap ~100 dimers at 180 s in 7 μM tubulin, k_l must be less than the elongation rate (18/s), but >18/s − 100/180 s = 17.4/s. This rate, however, produces a stable cap of 28,980 − (180 s × 17.4/s) = 25,848 dimers after 180 s at 23 μM tubulin, ~89% of the length of the microtubule and ~250 times greater than the value determined in our studies. At zero free tubulin, a cap of this size would persist for 25,848/(17.4 + 44) = 421 s. In support of the vectorial model, Carlier et al. (10) reported a maximum hydrolysis (and destabilization) rate of 40/s. If this value is correct, a plus end microtubule elongating for 180 s at 23 μM tubulin will be stabilized by a cap of 28,980 − (180 s × 40/s) = 21,780 subunits, which would persist for t = 21,780/(40 + 44) = 259 s at zero free tubulin. Clearly, the delays predicted by previously published hydrolysis rate values (9, 10, 25) far exceed the 3–4 s indicated by our results.

In contrast to the studies of Carlier and co-workers, other workers (27, 37, 41) have found that GTP hydrolysis and P_i release are tightly coupled to microtubule assembly. These

findings are consistent with the short life-time and size of the stable cap measured in our studies, and when combined with our results, provide strong support for some form of coupled destabilization mechanism, such as the stochastic dissociation, coupled hydrolysis model of O'Brien et al. (27) and Walker et al. (49) or the subsequent, "lateral cap" model of Bayley and co-workers (1). In coupled models, addition of new GTP-tubulin dimers to terminal GTP-tubulin subunits is thought to "force" their conversion to labile GDP-tubulin subunits as they become buried beneath the terminal layer. The probability of cap loss is thought to be mainly governed by cooperative interactions between terminal subunits modulated by competition between tubulin association and dissociation reactions (1, 27, 49). These reactions restrict the stable cap to the tip of an elongating end, independent of elongation rate and length, a prediction consistent with our results.

In Vivo Implications

Although most microtubules in vivo undergo the characteristic phases and transition of dynamic instability, the relationship between elongation rate and catastrophe frequency is not easily explained by in vitro data. Specifically, microtubules in vivo exhibit a high frequency of catastrophe at relatively high elongation rates. For example, the average rate of microtubule elongation in interphase newt lung cells is 7.2 μm/min and the average lifetime of elongation is 71 s (14). In contrast, a microtubule assembled from purified tubulin elongating at 7.2 μm/min will persist for >2,000 s (49) before catastrophe. How can microtubules in vivo convert to rapid shortening so frequently?

Our data show that microtubules elongating at high rates, independent of their length, will convert to rapid shortening within several seconds when the rate of tubulin association is inhibited by dilution below S_c^e. This result suggests that the cell could modulate catastrophe frequency by using molecules which transiently bind to elongating ends and suppress the rate of GTP-tubulin association in comparison to the rate of GTP-tubulin dissociation. Catastrophe frequency is stochastic (14, 19, 49) so that a number of transient events would probably be required before induction of catastrophe. Binding may not always induce catastrophe, only increase its probability; it is unlikely that a transient change in microtubule elongation rate over a few second period would be observed by video microscopy. Such "catastrophe promoters" would bind at low stoichiometry with low affinity and would be difficult to identify by conventional microtubule affinity methods (20, 40, 42).

We thank the members of the UNC-Duke microtubule journal club for their stimulating discussions and critical evaluation of this work. We are particularly indebted to Dr. Ken Jacobsen for the loan of the Berg-Block flow cell, and to Vicki Petrie and Susan Whitfield for technical and illustrative assistance.

Supported by National Institutes of Health grant GM 24364.

Received for publication 1 February 1991 and in revised form 25 March 1991.

References

1. Bayley, P. M., M. J. Schilstra, and S. P. Martin. 1990. Microtubule dynamic instability: numerical simulation of microtubule transition properties using a lateral cap model. *J. Cell Sci.* 95:33–48.
2. Bell, C. W., C. Fraser, W. S. Sale, W.-J. Y. Tang, and I. R. Gibbons. 1982. Preparation and purification of dynein. *Methods Cell Biol.* 24: 373–397.
3. Belmont, L. D., A. A. Hyman, K. E. Sawin, and T. J. Mitchison. 1990. Real time visualization of cell cycle dependent changes in microtubule dynamics in cytoplasmic extracts. *Cell.* 62:579–589.
4. Berg, H. C., and S. M. Block. 1984. A miniature flow cell designed for rapid exchange of media under high-power objectives. *J. Gen. Microbiol.* 130:2915–2920.
5. Caplow, M., and R. Reid. 1985. Directed elongation model for microtubule GTP hydrolysis. *Proc. Natl. Acad. Sci. USA.* 82:3267–3276.
6. Caplow, M., and J. Shanks. 1987. GTP requirement for in vitro and in vivo microtubule assembly and stability. *In* The Cytoskeleton in Cell Differentiation and Development. R. B. Maccioni and J. Arechaga, editors. IRL Press, Oxford, UK. 63–73.
7. Caplow, M., J. Shanks, and R. L. Ruhlen. 1988. Temperature-jump studies of microtubule dynamic instability. *J. Biol. Chem.* 263:10344–10352.
8. Caplow, M., R. Ruhlen, J. Shanks, R. A. Walker, and E. D. Salmon. 1989. Stabilization of microtubules by tubulin-GDP-P_i subunits. *Biochemistry.* 28:8136–8141.
9. Carlier, M.-F., and D. Pantaloni. 1981. Kinetic analysis of guanosine 5'-triphosphate hydrolysis associated with tubulin polymerization. *Biochemistry.* 20:1918–1924.
10. Carlier, M.-F., D. Didry, and D. Pantaloni. 1987. Microtubule elongation and guanosine 5'-triphosphate hydrolysis. Role of guanine nucleotides in microtubule dynamics. *Biochemistry.* 26:4428–4437.
11. Carlier, M.-F., D. Didry, R. Melki, M. Chabre, and D. Pantaloni. 1988. Stabilization of microtubules by inorganic phosphate and its structural analogs, the fluoride complexes of aluminum and beryllium. *Biochemistry.* 27:3555–3559.
12. Cassimeris, L., P. Wadsworth, and E. D. Salmon. 1986. Dynamics of microtubule depolymerization in monocytes. *J. Cell Biol.* 102:2023–2032.
13. Cassimeris, L. U., R. A. Walker, N. K. Pryer, and E. D. Salmon. 1987. Dynamic instability of microtubules. *Bioessays.* 7:149–154.
14. Cassimeris, L., N. K. Pryer, and E. D. Salmon. 1988. Real-time observations of microtubule dynamic instability in living cells. *J. Cell Biol.* 107:2223–2231.
15. Chen, Y., and T. L. Hill. 1985. Monte Carlo study of the GTP cap in a five-start helix model of a microtubule. *Proc. Natl. Acad. Sci. USA.* 82:1131–1135.
16. David-Pfeuty, T., H. P. Erickson, and D. Pantaloni. 1977. Guanosinetriphosphatase activity of tubulin associated with microtubule assembly. *Proc. Natl. Acad. Sci. USA.* 74:5372–5376.
17. Hayden, J. H., S. S. Bowser, and C. L. Rieder. 1990. Kinetochores capture astral microtubules during chromosome attachment to the mitotic spindle: direct visualization in live newt lung cells. *J. Cell Biol.* 111:1039–1046.
18. Hiller, G., and K. Weber. 1978. Radioimmune assay for tubulin: a quantitative comparison of the tubulin content of different established tissue culture cells and tissues. *Cell.* 14:795–804.
19. Horio, T., and H. Hotani. 1986. Visualization of the dynamic instability of individual microtubules by dark-field microscopy. *Nature (Lond.).* 321:605–607.
20. Kellogg, D. R., C. M. Field, and B. M. Alberts. 1989. Identification of microtubule-associated proteins in the centrosome, spindle, and kinetochore of the early *Drosophila* embryo. *J. Cell Biol.* 109:2977–2991.
21. Kirschner, M., and T. Mitchison. 1986. Beyond self-assembly: from microtubules to morphogenesis. *Cell.* 45:329–342.
22. Kirschner, M. W., and T. Mitchison. 1986. Microtubule dynamics. *Nature (Lond.).* 324:621.
23. Kobayashi, T. 1975. Dephosphorylation of tubulin-bound guanosine triphosphate during microtubule assembly. *J. Biochem. (Tokyo).* 77:1193–1197.
24. Leslie, R. J., W. M. Saxton, T. J. Mitchison, B. Neighbors, E. D. Salmon, and J. R. McIntosh. 1984. Assembly properties of fluorescein-labeled tubulin in vitro before and after fluorescence bleaching. *J. Cell Biol.* 99:2146–2156.
25. Melki, R., M.-F. Carlier, and D. Pantaloni. 1990. Direct evidence of GTP and GDP-Pi intermediates in microtubule assembly. *Biochemistry.* 29: 8921–8932.
26. Mitchison, T., and M. Kirschner. 1984. Dynamic instability of microtubule growth. *Nature (Lond.).* 312:237–242.
27. O'Brien, E. T., W. A. Voter, and H. P. Erickson. 1987. GTP hydrolysis during microtubule assembly. *Biochemistry.* 26:4148–4156.
28. Pantaloni, D., and M.-F. Carlier. 1986. Involvement of guanosine triphosphate (GTP) hydrolysis in the mechanism of tubulin polymerization: regulation of microtubule dynamics at steady state by a GTP cap. *Ann. NY. Acad. Sci.* 466:496–509.
29. Rieder, C. L., and S. P. Alexander. 1990. Kinetochores are transported poleward along a single astral microtubule during chromosome attachment to the spindle in newt lung cells. *J. Cell Biol.* 110:81–95.
30. Rieder, C. L., E. A. Davison, L. C. W. Jensen, L. Cassimeris, and E. D. Salmon. 1986. Oscillatory movements of monooriented chromosomes and their position relative to the spindle pole result from the ejection properties of the aster and half-spindle. *J. Cell Biol.* 103:581–591.
31. Salmon, E. D. 1989. Metaphase chromosome congression and anaphase

poleward movement. *In* Cell Movement. Vol. 2. Kinesin, dynein, and microtubule dynamics. F. D. Warner and J. R. McIntosh, editors. Alan R. Liss, Inc., New York. 431–440.
32. Salmon, E. D. 1989. Microtubule dynamics and chromosome movement. *In* Mitosis. J. S. Hyams and B. R. Brinkley, editors. Academic Press, Inc., New York. 119–181.
33. Salmon, E. D., and P. Wadsworth. 1986. Fluorescence studies of tubulin and microtubule dynamics in living cells. *In* Applications of Fluorescence in the Biomedical Sciences. D. L. Taylor, A. S. Waggoner, R. F. Murphy, F. Lanni, R. R. Birge, editors. Alan R. Liss, Inc., New York. 377–403.
34. Sammak, P. J., and G. G. Borisy. 1988. Direct observation of microtubule dynamics in living cells. *Nature (Lond.).* 332:724–726.
35. Sammak, P. J., G. J. Gorbsky, and G. G. Borisy. 1987. Microtubule dynamics in vivo: a test of mechanisms of turnover. *J. Cell Biol.* 104: 395–405.
36. Saxton, W. M., D. L. Stemple, R. J. Leslie, E. D. Salmon, M. Zavortink, and J. R. McIntosh. 1984. Tubulin dynamics in cultured mammalian cells. *J. Cell Biol.* 99:2175–2186.
37. Schilstra, M. J., S. R. Martin, and P. M. Bayley. 1987. On the relationship between nucleotide hydrolysis and microtubule assembly: studies with a GTP-regenerating system. 147:588–595.
38. Schulze, E., and M. Kirschner. 1986. Microtubule dynamics in interphase cells. *J. Cell Biol.* 102:1020–1031.
39. Schulze, E., and M. Kirschner. 1988. New features of microtubule behavior observed in vivo. *Nature (Lond.).* 334:356–359.
40. Sloboda, R. D., and J. L. Rosenbaum. 1982. Purification and assay of microtubule-association proteins (MAPs). *Methods Enzymol.* 85:409–416.
41. Stewart, R. J., K. W. Farrell, and L. Wilson. 1990. Role of GTP hydrolysis in microtubule polymerization: evidence for a coupled hydrolysis mechanism. *Biochemistry.* 29:6489–6498.
42. Vallee, R. B., and C. A. Collins. 1986. Purification of microtubules and microtubule-associated proteins from sea urchin eggs and cultured mammalian cells using taxol, and use of exogenous taxol-stabilized brain microtubules for purifying microtubule-associated proteins. *Methods Enzymol.* 134:116–127.
43. Verde, F., J. Labbé, M. Doree, and E. Karsenti. 1990. Regulation of microtubule dynamics by cdc2 kinase in cell free extracts of *Xenopus* eggs. *Nature (Lond.).* 343:233–238.
44. Voter, W. A., and H. P. Erickson. 1984. The kinetics of microtubule assembly. *J. Biol. Chem.* 259:10430–10438.
45. Deleted in proof.
46. Voter, W. A., E. T. O'Brien, and H. P. Erickson. 1991. Dilution-induced disassembly of microtubules: relation to dynamic instability and the GTP cap. *Cell Motil. Cytoskeleton.* 18:55–62.
47. Wadsworth, P., and E. D. Salmon. 1986. Microtubule dynamics in mitotic spindles of living cells. *Ann. NY Acad. Sci.* 466:580–592.
48. Wadsworth, P., and E. D. Salmon. 1986. Preparation and characterization of fluorescent analogs of tubulin. *Methods Enzymol.* 134:519–528.
49. Walker, R. A., E. T. O'Brien, N. K. Pryer, M. Soboeiro, W. A. Voter, H. P. Erickson, and E. D. Salmon. 1988. Dynamic instability of individual microtubules analyzed by video light microscopy: rate constants and transition frequencies. *J. Cell Biol.* 107:1437–1448.
50. Walker, R. A., S. Inoué, and E. D. Salmon. 1989. Asymmetric behavior of severed microtubule ends after ultraviolet-microbeam irradiation of individual microtubules in vitro. *J. Cell Biol.* 108:931–937.
51. Weisenberg, R. C., W. J. Deery, and P. J. Dickinson. 1976. Tubulin-nucleotide interactions during polymerization and depolymerization of microtubules. *Biochemistry.* 15:4248–4254.